ACS OMEGA

Open Access

http://pubs.acs.org/journal/acsodf

Article

Zeolite Functionalized with Magnesium/Aluminum/Lanthanum Ternary Hydroxide for the Phosphometabolite Profiling of Malignant Neoplastic Serum Samples

Tasbiha Malik, Batool Fatima,* Dilshad Hussain, Fahmida Jabeen, Shan E Zahra Jawad, Abrar Mohyuddin, and Muhammad Najam-ul-Haq*

Cite This: *ACS Omega* 2024, 9, 31335−31343

Read Online

ACCESS | Metrics & More | Article Recommendations | Supporting Information

ABSTRACT: ATP upregulation is a significant driver of aggressive cancer cell phenotypes. Phosphometabolites participate in metabolic pathways and are overexpressed in cancer cell activity. Therefore, developing novel and accurate methods for detecting phosphometabolites in biological fluids is essential. In this research, a novel zeolite composite comprising magnesium, aluminum, and lanthanum hydroxides (MALZ) is developed and used for the first time to enrich phosphorylated metabolites via its inherent interaction with phosphate groups. SEM micrographs show a crystalline cubic structure with a small diameter of 36.62 nm. FTIR analysis confirms the phosphate adsorption and desorption using AMP and ATP as the standards. XRD analysis of MALZ provides structural information about the synthesized composite. Adsorption−desorption parameters, such as pH, shaking time, and MALZ concentration, are optimized to analyze the binding capacity of the fabricated material for phosphorylated metabolites. A kinetic study reveals the rapid and effective AMP and ATP adsorptions on MALZ. The multiple hydroxyl groups of ternary hydroxides and high affinity of lanthanum toward the phosphate group enrich 26 phosphometabolites from serum samples of malignant neoplastic patients. The LC−MS profile shows characteristic phosphometabolites that may act as signatures of cancer-related abnormal metabolic pathways. This study may provide an experimental pathway for detecting metabolites in human body fluids.

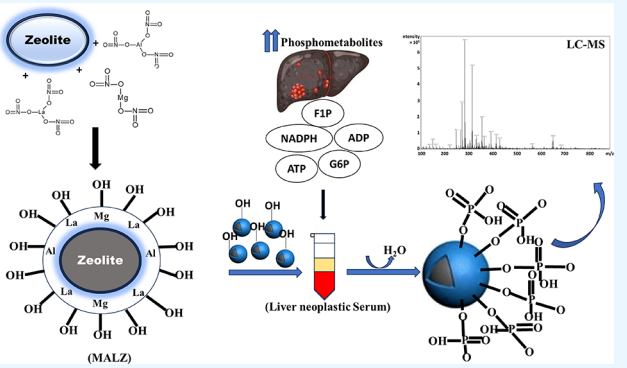

1. INTRODUCTION

Energy is necessary for the production and functioning of biomolecules. Therefore, cancer cells need ATP to maintain their growth.[1] Several post-translational modifications (PTMs) influence NF-β signaling including phosphorylation. It is the common PTM type in NF-κB signaling and contributes to cancer progression.[2] Protein and lipid metabolisms can be altered by a change in energy supply via the AMP-activated protein kinase (AMPK). The clinicopathological significance of AMPK in breast cancer shows that AMPK expression levels in triple-negative breast cancer (TNBC) are higher than those in non-triple-negative breast cancer (NTNBC) cells. Moreover, AMPK is upregulated in TNBC tissues compared to NTNBC.[3]

The cellular plasma membrane takes up metabolites processed in the cytoplasm. It is then transported to intracellular organelles, i.e., peroxisomes and mitochondria, for further processing as they are considered the central points for cancer cell metabolism.[4] Adenosine triphosphate (ATP) and guanosine triphosphate (GTP) are the purine nucleotides for DNA and RNA syntheses and energy metabolism. The biosynthesis of purine nucleotides is increased in malignant tumors because of their high proliferation. Cancer cells upregulate inosine monophosphate dehydrogenase (IMPDH), the rate-limiting enzyme in de novo GTP biosynthesis. De novo synthesis of GMP (guanosine monophosphate) is also regulated by this enzyme. These phosphometabolites are higher in cancer cells than in normal cells.[5] Cancer metastasis and angiogenesis are promoted by adenosine diphosphate (ADP), thus being a target to diagnose and treat cancer.[6]

Liver cancer is the most common cancer leading to death because of poor prognosis, and its prognosis is dismal as it is discovered at a late stage.[7] Protein kinase depletion in hepatocytes facilitates liver cancer progression, which promotes autophagy and oxidative phosphorylation.[8] Cellular

Received: October 31, 2023
Revised: March 2, 2024
Accepted: April 1, 2024
Published: July 9, 2024

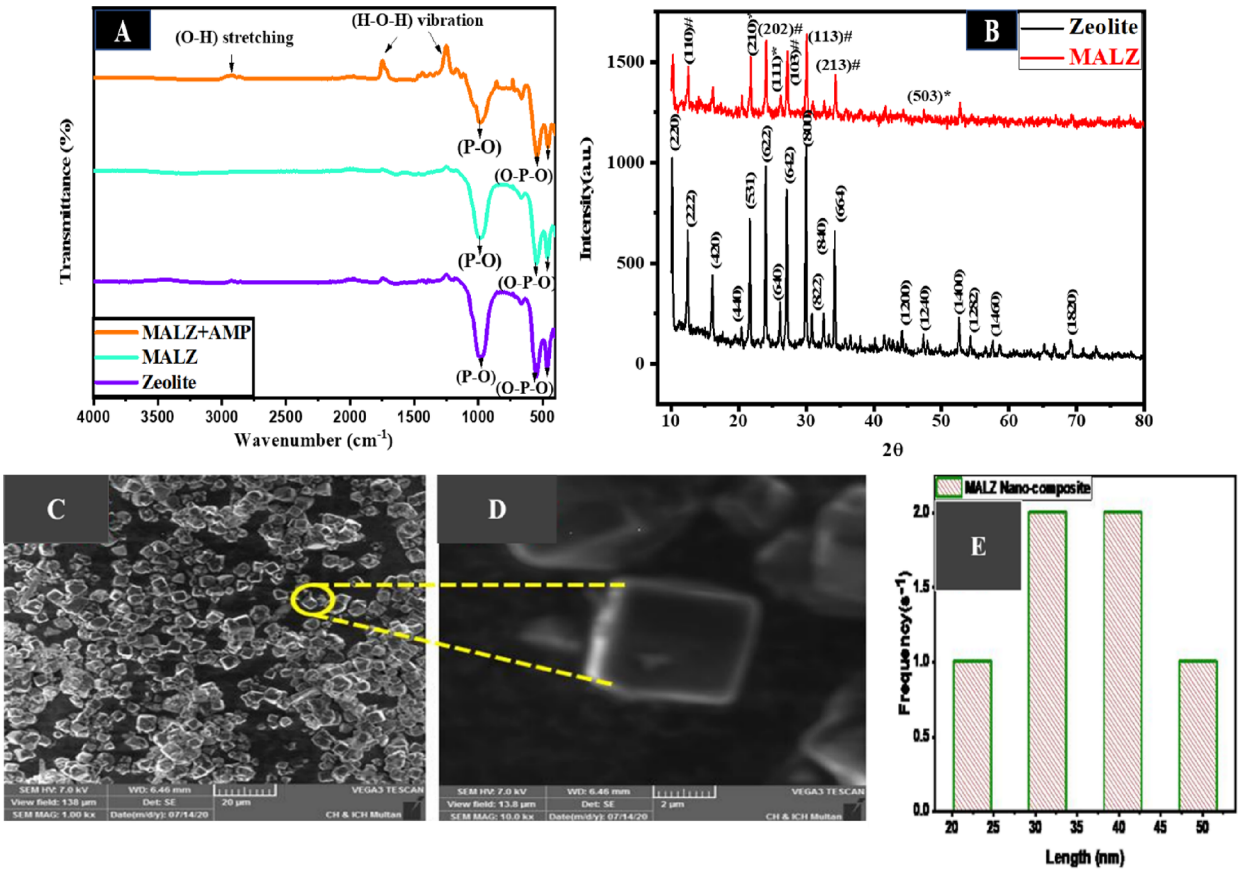

Figure 1. (A) FTIR spectra of zeolite, MALZ without and with phosphate adsorption, (B) XRD crystallographic analysis of precursor zeolite and MALZ, (C, D) SEM micrographs of MALZ at different magnification levels, and (E) particle size distribution of Zeolite@MALZ represented via histogram.

ATP and ADP levels are elevated in liver cancer. The ATP to ADP ratio differs in cancer cells than in normal cells.[9,10] Some genes dephosphorylate extracellular ATP to ADP and AMP by extracellularly releasing ATP in liver cancer.[11] Cancer cells increase their proliferation as the phosphometabolites build up.[12] ATP upregulation in cancer cells enhances several aggressive behaviors, i.e., migration, stemness, anchorage independence, drug resistance, antioxidant capacity, and cell proliferation.[13]

Various enrichment approaches in phospho-proteomics have been used to enrich phosphoproteins and phospho-peptides selectively. Frequently employed enrichment techniques include immunoprecipitation, coprecipitation, ion exchange chromatography, chemical derivatization, immobilized metal affinity chromatography (IMAC), metal oxide chromatography (MOAC), inorganic salt affinity chromatography, and coprecipitation. IMAC is based on the affinity of phosphate groups for metal ions such as Cu^{2+}, Ni^{2+}, Zn^{2+}, and Fe^{3+}.[14] Fe^{3+} and Ga^{3+} are often utilized, and TiO2 is often used in MOAC and has a high affinity for p-peptides. Cerium-based nanocomposites allow the simultaneous study of mono- and multipeptides.[15] Fe^{3+}, Zr^{4+}, Ti^{4+}, Al^{3+}, La^{3+}, and Ga^{3+} have distinctive characteristics and better selectivity for phosphorylated biomolecules.[16] La_2O_3 nanoparticles have a powdery nature.[17] Enhanced enrichment of monophosphorylated peptides is seen for alumina-zirconia.[16]

Wang et al. recorded serum metabolic fingerprinting (SMF) by employing nanoparticle-enhance laser desorption/ionization mass spectrometry (NPELDI MS) for the "one-stop shop" diagnosis of polycystic ovary syndrome (PCOS).[18] In a comprehensive review by Li et al., the utilization of bionanoparticles, i.e., exosomes, virus nanoparticles, nucleic acid nanoparticles, and protein nanoparticles, as nanomedicine for cancer diagnosis, imaging, and treatment is discussed.[19] Lung cancer, kidney cancer, and liver cancer were diagnosed in a recent study by employing Fe-MOF-UL by engineering at the atomic, i.e., metal node of Fe/Co/Ni, and supermolecular level, i.e., ultrathin/bulk. SMF metabolic signals were extracted using 0.1 μL of serum per sample.[20] Huang et al. utilized NPELDI MS to record SMF for diagnosis and prognosis of breast cancer (BrCa). SMF machine learning is an efficient readout to differentiate non-BrCa from BrCa.[21]

In this study, magnesium, aluminum, and lanthanum ternary hydroxides are loaded on zeolite to prepare a MALZ (Mg-Al-La-zeolite) composite and used to enrich phosphorylated metabolites. After parameter optimizations, the comprehensive analysis of phosphorylated metabolites in liver cancer serum samples is carried out via liquid chromatography−mass spectrometry (LC−MS). The MALZ composite can efficiently capture phosphorylated metabolites because of its inherent interaction with the phosphate groups. The main objective of this proposed study is to evaluate the modification of zeolite for efficient phosphometabolite adsorption and desorption. This study may lead to the development of novel detection methods for phosphorylated and other metabolites.

https://doi.org/10.1021/acsomega.3c08610
ACS Omega 2024, 9, 31335−31343

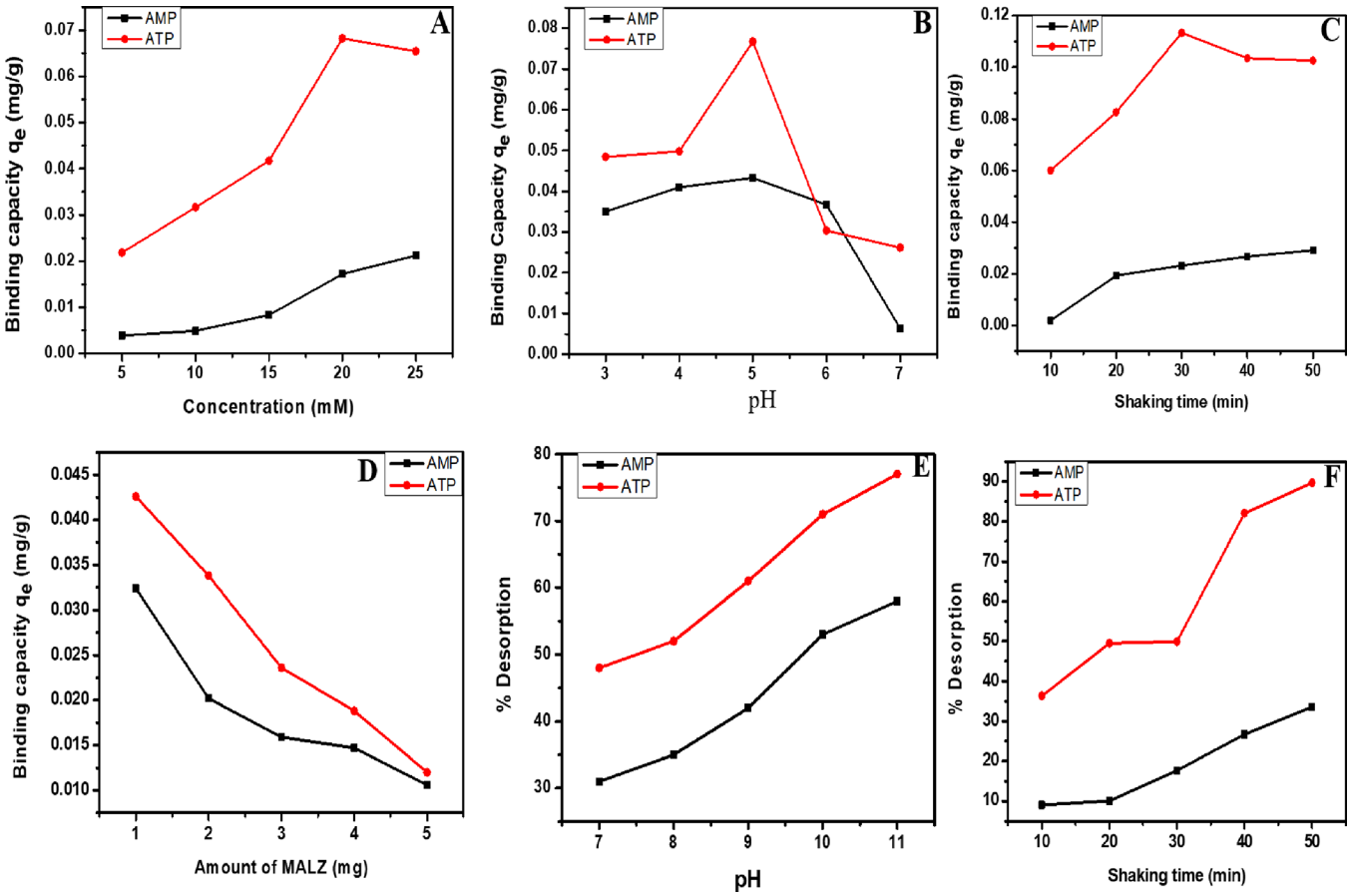

Figure 2. Graphical representation of parameters indicating the binding capacity of Zeolite@MALZ with AMP and ATP at (A) different concentrations, (B) pH, (C) incubation time, (D) amount of Zeolite@MALZ, (E) desorption pH, and (F) desorption time. (Comprehensive exploration of the binding capacity of synthesized material with ATP and AMP provides information about the effects of varying concentration, pH, and incubation times. Zeolite@MALZ concentration, desorption pH, and time provide an understanding of adsorption−desorption dynamics and optimal conditions for removing analytes.)

2. EXPERIMENTAL SECTION

2.1. Reagents and Materials. *2.1.1. Preparation of MALZ.* A coprecipitation method[22] was used to prepare magnesium−aluminum−lanthanum ternary hydroxides loaded on porous zeolite. Magnesium nitrate hexahydrate, aluminum nitrate nanohydrate, and lanthanum nitrate were added to 200 mL of deionized water, wherein magnesium and lanthanum nitrates had twice the molar ratio than aluminum nitrate. In the second step, 10 g of porous zeolite (sodium aluminosilicate hydrate) was added and stirred for 3 h at room temperature. The reaction mixture was added with 28% ammonia solution until the pH reached 9.5 and stirred for 3 h. Precipitates were kept for 24 h at room temperature. The solid was collected and washed using ultrapure water until the filtrate's pH became neutral. The washed precipitates were dried for 24 h in an oven at 65 °C. Prepared MALZ was pulverized to a fine powder followed by drying and dehydrating at 400 °C.

2.1.2. Solid Phase Extraction (SPE) of Phosphorylated Metabolites. Adsorption−desorption studies were carried out using AMP and ATP as standards. For 0.1 M AMP solution, 1.8 g of AMP was dissolved in 50 mL of deionized water. Similarly, 0.1 M ATP solution was prepared by dissolving 336 mg in 10 mL of deionized water. After dilution, the solutions were sonicated for 20 min, and absorbance was recorded at 259 nm.

2.1.3. Parameter Optimization. The binding capacity of MALZ was optimized for evaluating parameters such as the effect of AMP and ATP concentrations, pH, shaking time, and amount of the enrichment material. Experimental details are provided in the Supporting Information.

2.1.4. Effect of pH on Desorption. Desorption of bound AMP was carried out to estimate the ability of MALZ to enrich phosphate moieties. After desorption, MALZ can be reused for several cycles. The desorption experiment was similar to dephosphorylation, and the effects of pH and shaking time were optimized for the serum analysis. The details are given in the Supporting Information.

2.1.5. LC−MS Analysis. Serum samples of liver cancer patients were taken with the prior consent of the Ethical Committee of Nishtar Hospital Multan, Pakistan, and stored at −20 °C. Proteins were precipitated by acetonitrile and centrifuged at 14,000*g*, and the protein pellet was removed. The liquid samples were filtered to remove any particulate matter. MALZ (10 mg) was used to enrich under the optimized conditions. The acidic pH was adjusted to 5, and the sample was shaken at 25 °C for 30 min at 140 rpm. After the sample loading, the material was washed and filtered. For elution, the pH was brought to 11 and further shaken for 30 min, and the filtrates were collected and analyzed by LC-ESI-MS analysis.

https://doi.org/10.1021/acsomega.3c08610
ACS Omega 2024, 9, 31335−31343

3. RESULTS AND DISCUSSION

Zeolites act as ion exchangers and have a high loading capacity due to their high surface area. Magnesium, aluminum, and lanthanum zeolites are designed to capture phosphorylated molecules from standard and serum samples. Magnesium ions bind phosphate groups at neutral and acidic pH. La has a similar affinity for phosphate as Al3+, and the latter binds with ATP and other phosphorylated molecules more strongly than Mg^{2+} and Ca^{2+}. The phosphate binds at the terminal phosphate, thus promoting GTP, AMP, and ADP bindings.

3.1. Characterization of MALZ. The phosphate binding potential of MALZ is characterized by FTIR analysis. Figure 1A represents the FTIR spectra of raw zeolite and MALZ before and after adsorption of AMP. Zeolite shows characteristic peaks at 1747, 1249, and 661 cm^{-1}. A similar peak pattern is observed for MALZ with 1247 and 670 cm^{-1} peaks. MALZ after phosphate adsorption shows peaks at 2925, 1739, 1253, 982, 670, 548, and 464 cm^{-1}. The peaks between 1200 and 1800 cm^{-1} show hydroxyl groups. Peaks around 464, 548, and 661 cm^{-1} are attributed to phosphate complexes, i.e., $LaPO_4$ and $AlPO_4$. A bending at 982 cm^{-1} is due to the asymmetric stretch of the P−O bond. Hence, FTIR spectra confirm AMP enrichment via the hydroxyl groups of MALZ.

MALZ and its precursor zeolite are investigated for crystallographic structures and solid-state chemistry through X-ray diffraction. Figure 1B represents the diffraction peaks at 2θ of 12, 21, 23, 25, 26, 29, 34, and 47°, indicating the crystallographic frames of (110) $La(OH)_3$, (210) La_2O_3, (202) $La(OH)_3$, (111) La_2O_3, (103) $La(OH)_3$, (113) $La(OH)_3$, (213) $La(OH)_3$, and (503) La_2O_3, respectively. The data are consistent with the literature and JCPDS database SD card number 01-089-8015. Small peaks show the impurities of salts and other byproducts. The zeolite provides a solid support where lanthanum hydroxide and lanthanum oxide intermediates are impregnated. No diffraction peaks are observed for Al and Mg because of their low stoichiometric quantities and higher dispersion of La in the MALZ.

MALZ's surface morphology and size are examined using scanning electron microscopy (SEM). Figure 1C,D shows a cubic morphology with uniform adsorption on the zeolite surface. The observed average MALZ size is ∼36.62 nm,[23] indicating that a large surface area can bind maximum phosphate molecules. Figure 1E represents a histogram that indicates the particle size distribution of the synthesized zeolite, and the calculated polydispersity index (PDI) is 0.14.

This study aims to attach phosphorylated metabolites because the synthesized composite possesses an inherent interaction capability for phosphate groups. As reported in a recent study, lanthanum on MALZ supports phosphate attachment, as La is a hard electron acceptor with a preference for oxygen-containing anions. Moreover, zeolite, aluminum, and magnesium-based materials have also been reported for phosphate adsorption.[23−25]

3.2. Adsorption Studies. *3.2.1. Effect of AMP and ATP Concentrations on MALZ Enrichment Capacity.* Adenosine monophosphate (AMP) and adenosine triphosphate (ATP) are standard phosphorylated metabolites to optimize the enrichment parameters such as analyte concentration, pH, shaking time, and MALZ amount. First, different concentrations of standards are prepared and enriched using the MALZ composite. Figure 2A indicates a linear relationship between the AMP and ATP concentrations and MALZ binding capacity. The concentrations of AMP and ATP vary from 5 to 25 mM at room temperature, pH 5, and the amount of MALZ = 5 mg. Figure 2A describes the adsorptions of ATP and AMP as a function of their concentrations. Increasing the concentration increases the enriched amounts of ATP and AMP from the solution, attributed to the higher availability of exchangeable and active phosphate molecules to combine with surface hydroxyl groups of MALZ, resulting in an elevated desorption efficiency or binding capacity of MALZ.

3.2.2. Effect of pH on the Binding Efficiency of MALZ. The binding capacity of MALZ is then evaluated at different pH values of standard solutions. The binding efficiency of MALZ increases in acidic pH up to 5 and decreases as the pH gets neutral. Results are aligned to the concept of protonation of OH^- groups under acidic conditions. In the pH range 2−5, there are more H^+ ions in the solution to protonate OH groups on MALZ, introducing a strong positive charge on MALZ. This positive charge attracts the negatively charged phosphate of AMP for adsorption on MALZ through electrostatic interactions. At pH 6−7, H^+ ions decrease as maximum phosphate is adsorbed, and OH− groups from the surface are removed and clustered in the solution. A pool of OH^- and phosphate ions is created, and competition among negatively charged ions is developed for attachment to the adsorbent. It hinders the overall adsorption capacity of MALZ at a higher pH of 6−7.[26,27] Therefore, the binding capacity peaks at pH 5, and this trend is observed in Figure 2B.

3.2.3. Effect of Shaking Time on the Binding Capacity of MALZ. The effect of shaking time on the attachment of AMP (15 mM) and ATP (15 mM) on 5 mg of MALZ is investigated at pH 5 by varying shaking time from 10 to 50 min. Results in Figure 2C indicate that MALZ binding capacity increases from 0.0019 to 0.0291 mg/g for AMP and 0.0599 to 0.10344 mg/g for ATP as the shaking time increases from 10 to 50 min with 10 min intervals. A small decrease in binding capacity is observed at higher shaking times. A possible explanation for the increase is that as the shaking time increases, there is more time for the protonated positively charged surface hydroxyl groups of MALZ to interact with negatively charged phosphates of AMP and ATP in the solution. A slight decrease in binding capacity with increasing shaking time may be due to the saturation of surface OH^- groups of MALZ.

3.2.4. Effect of MALZ Amount on Enrichment. Results reflect a uniform decrease in the binding capacity, and this trend shows a negative correlation between the MALZ amount and its binding capacity. MALZ's surface area is high because of its small size, leading to higher phosphate enrichment. A small MALZ amount is sufficient to adsorb higher phosphate concentration. Only 1 mg MALZ has enough binding sites to adsorb AMP and ATP from the 15 mM solution used in these experiments.[28]

AMP and ATP concentrations adsorbed on MALZ are calculated using the binding capacity equation:[29]

$$(q_e) = (C_o - C_{eq}) \times m/V$$

where q_e is the binding capacity of MALZ, C_o is the AMP and ATP concentrations in the blank before adsorption, C_{eq} is the AMP and ATP concentrations in the solution after enrichment, m is the mass of MALZ, and V is the volume of AMP solution.

3.3. Desorption Parameters. *3.3.1. Effect of pH on Desorption.* Desorption is calculated in percentage using the following formula:

https://doi.org/10.1021/acsomega.3c08610
ACS Omega 2024, 9, 31335−31343

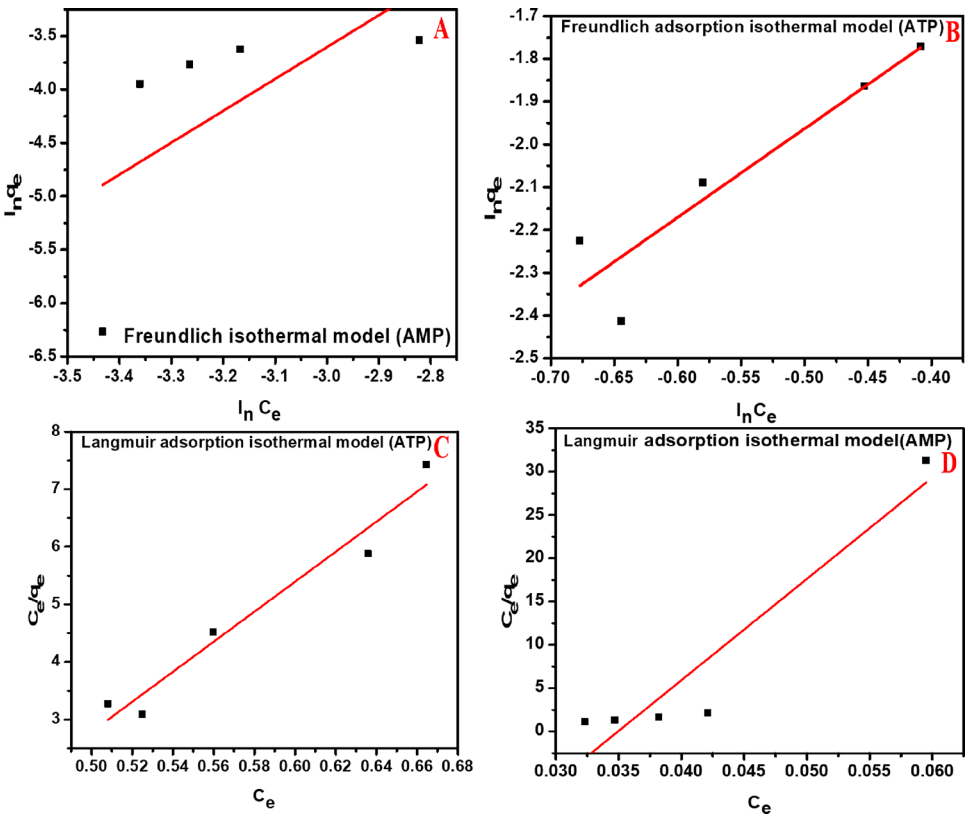

Figure 3. Adsorption kinetics for MALZ at initial AMP and ATP concentrations. Freundlich model for (A) AMP and (B) ATP and Langmuir model for (C) ATP and (D) AMP. (Investigation of adsorption kinetics coupled with Langmuir and Freundlich models of MALZ for ATP and AMP provides a comprehensive understanding of sorption activity, resulting in valuable details of adsorption mechanisms and surface interaction characteristics between modified zeolite material and adsorbate molecules.)

$$R_D = (C_D \times V_D/q_e \times m) \times 100$$

where R_D is the percentage desorption, C_D is the concentration of desorbed AMP as calculated from absorbance using Beer's law, V_D is the volume used from the desorption procedure, q_e is the optimum binding capacity under optimum conditions, and m is the amount of MALZ. Here, V_D is 3 mL; q_e is constant, i.e., 0.0433; and m is 5 mg.

The pH has an essential role in analyte enrichment and in its elution or desorption. Enrichment is facilitated under acidic conditions, as discussed above. In contrast, desorption occurs under basic conditions as more hydroxyl groups are available in the solution to compete with AMP and ATP phosphate groups in reaching the MALZ surface. At higher pH values, the protonated OH groups are deprotonated, which disturb the electrostatic interactions between MALZ and phosphorylated metabolites. Therefore, these metabolites are released in the solution. Figure 2 (E) shows a linear increase in the desorption of AMP and ATP at higher pH. These results are consistent with the previous studies on phosphorylated biomolecule enrichment using nanomaterials.

3.3.2. Effect of Shaking Time on Desorption. The effect of the shaking time on AMP and ATM desorption is also evaluated. Figure 2E illustrates the linear increase in MALZ desorption efficiency with increasing shaking time. Under basic conditions (pH 11), the desorption efficiency increases by increasing shaking time from 10 to 50 min with 10 min intervals. The increase in the desorption percentage is due to the availability of more time for hydroxyl groups present in the basic solution to interact with MALZ having enriched phosphate groups of AMP and ATP.

3.4. Kinetics and Thermodynamics Studies. *3.4.1. Pseudo-First-Order Model.* The Lagergren rate equation explains the phosphate enrichment process, which can be presented in the pseudo-first-order. Enriching adsorbate from liquid solution has a proportionality relationship between occupied sites on the adsorbent and unoccupied sites. The equation for this model is given below:

$$dq_t/\mathrm{dt} = \mathrm{k1}(q_e - q_t)$$

Taking integrals on both sides of the equation, at times 0 to t and adsorption capacities 0 to qt, the equation is obtained as below:

$$\mathrm{Log}(q_e - q_t) = \log q_e - (\mathrm{k1}/2.303)\mathrm{t}$$

where q is the enriched amount of AMP and ATP (mg/g), subscripts t and q denote the state at equilibrium and time t (min), respectively, and k1 is the rate constant. By plotting the graph between the script (t) on the x axis and ln(qe−qt) on the y axis, the slope is described in terms of the rate constant of the pseudo-first-order model as depicted in Figure S1A.

3.4.2. Pseudo-Second-Order Model. The second order describes the adsorption kinetics mechanism, and a general assumption from the pseudo-order model is that the process of adsorption increases at first, decreases with time, and becomes constant. This model best explains chemical equilibrium and nonphysical equilibrium. The rate equation for the pseudo-second-order model is given below:

https://doi.org/10.1021/acsomega.3c08610
ACS Omega 2024, 9, 31335−31343

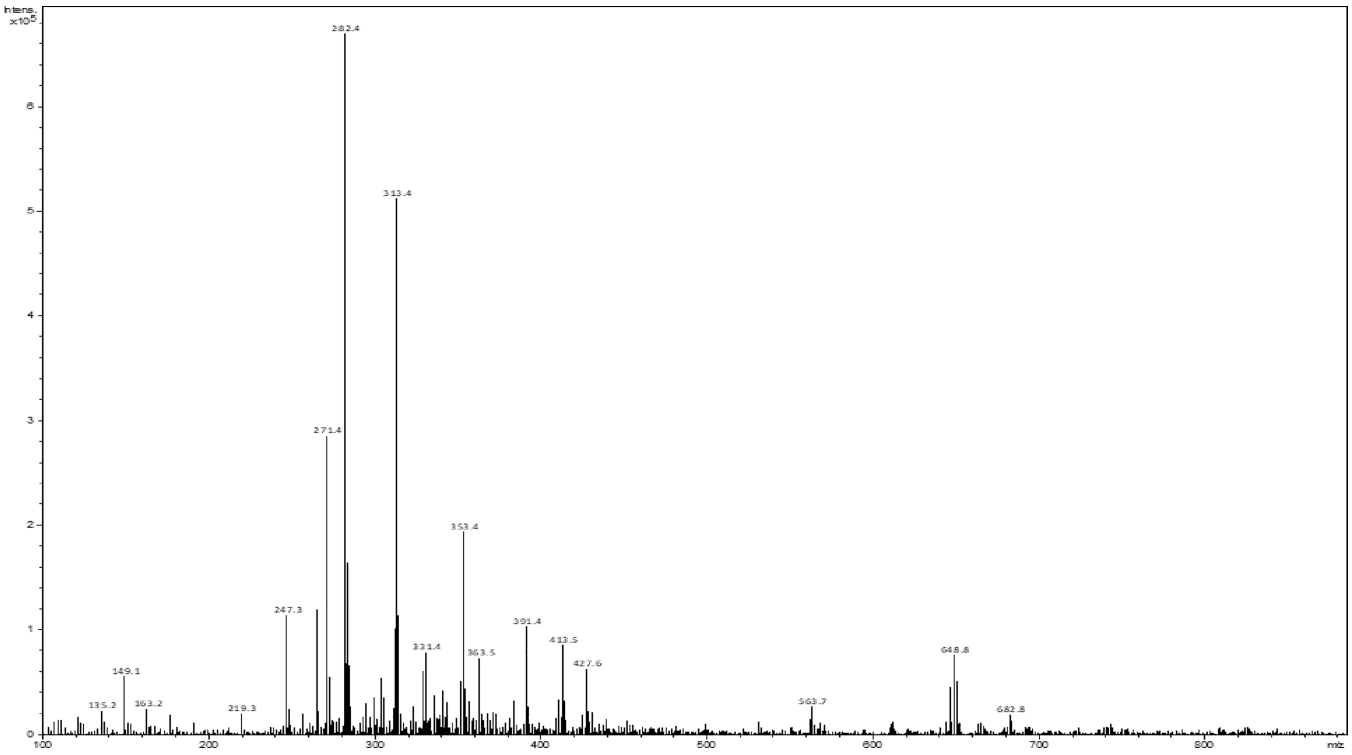

Figure 4. MS profile of detected phosphometabolites enriched from malignant neoplastic samples by MALZ via SPE followed by LC−MS. (Mass spectrometry profiles of phosphometabolites indicate the presence of specific phosphorus-containing compounds, providing a specific and targeted approach for discovering potential biomarkers and deeper insights into metabolic changes associated with malignancy.)

$$dq_t/\mathrm{dt} = \mathrm{k}_2(q_e - q_t)^2$$

Similarly, an integrated linear equation for the pseudo-second-order can be obtained as follows:

$$\mathrm{t}/q_t = 1/\mathrm{k}_2 \cdot \mathrm{q}^2\mathrm{e} + (1/q_e)\mathrm{t}$$

By plotting the graph between time t on the x axis and t/qt on the y-axis, the rate constant for the pseudo-second-order can be calculated, as shown in Figure S1C.

3.4.3. Intraparticle Diffusion Model. The chances of AMP and ATP to travel into MALZ pores are explained by the intraparticle diffusion model. The equation describing this model is given below:

$$q_t = k_{di}t^{1/2} + C_i$$

where k_{di} [g/(mg·min 0.5)] is the adsorption rate constant of the intraparticle diffusion model and C_i (mg/g) is a constant related to boundary layer thickness. The graph is plotted between $t^{1/2}$ on the x axis, q_t on the y axis, and k_{di} is the slope for the intraparticle diffusion model.

The graph is linearly plotted if intraparticle diffusion is involved in the enrichment. If the plotted line does not pass through the origin, it indicates that some other mechanism is involved in the enrichment. The graph suggests that the plot does not pass through the origin, and some other mechanism controls the enrichment process.[30] Table S1 indicates that the R^2 trend is as follows: intraparticle diffusion (R^2) < pseudo-first-order (R^2) < pseudo-second-order (R^2).

The trend suggests that the enrichment of both AMP and ATP is of pseudo-second-order. The pseudo-second-order model describes that the adsorption of AMP and ATP is parallel to the number of free active sites on MALZ and gives the maximum value at complete saturation and formation of one complete layer of AMP and ATP on the MALZ surface.[31]

3.4.4. Freundlich Isothermal Adsorption Model. The Freundlich isothermal adsorption model is an empirical equation based on heterogeneous surfaces of materials. The linear equation is expressed as

$$\log q_e = \log k + \frac{1}{n}(\log C_e)$$

where C_e is the concentration at equilibrium (mg/L), n is the exponential constant for the Freundlich equation expressing energy heterogeneity of enriched surface, and k is the Freundlich constant showing the relative enrichment capacity of MALZ.

The results of AMP and ATP enrichment by MALZ using the Freundlich adsorption isothermal model are shown in Figure 3A,B.

3.4.5. Langmuir Adsorption Isothermal Model. The enrichment isotherms of ATP and AMP on MALZ at 25 °C and pH 5 are shown in Figure 3C,D, respectively, using the following formula:

$$q_e = q_m \frac{(K_L C_e)}{1} + K_L C_e$$

where q_m (mg/g) is the enrichment capacity and K_L (L/mg) is the Langmuir constant.

From Table S2, R^2 values for the Langmuir model are higher than those of Freundlich for both AMP and ATP; thus, experimental results best fit the Langmuir isothermal model.

3.5. Serum Phosphometabolite Analysis. The metabolic traits of malignant liver cancer focus on three metabolic alterations: glycolysis, lipid metabolism, and glutamine addiction. As serum metabolome reflects the patient's body

https://doi.org/10.1021/acsomega.3c08610
ACS Omega 2024, 9, 31335−31343

Table 1. Identified Phosphorylated Metabolites after Enrichment with MALZ followed by LC−MS Analysis of Control and Malignant Neoplastic Serum Samples[a]

sr. no.	monoisotopic mass	phosphorylated metabolite	HMDB ID	metabolic pathway Involved
1	149.1	*O*-phosphoethanolamine	HMDB0000224	accumulation in cancer cells during glutamine deprivation correlated with tumor growth under nutrient starvation
2	169.1	phosphoenol pyruvate	HMDB0000263	inhibited cell growth, proliferation, migration, invasion, and induced robust apoptosis activation
3	200.1	4-*O*-phosphono-D-erythrose	HMDB0001321	involved in a metabolic disorder called glucose-6-phosphate dehydrogenase deficiency pathway
4	244.03	fucose 1-phosphate	HMDB0001265	hyperactivity of glycolysis
5	257.10	**glycerophosphocholine**	HMDB0000086	overexpression in cancer cells
6	260.02	glucose 6-phosphate	HMDB0001401	hyperactivity of glycolysis
7	265.95	glyceric acid 1,3-biphosphate	HMDB0001270	involved in the Warburg effect (aerobic glycolysis), a metabolic shift as a cancer hallmark
8	300.1	2-trans,-6-trans-farnesyl monophosphate	HMDB0304088	
9	313.4	5′-phosphoribosyl-*N*-formyl glycin amidine	HMDB0002305	biochemical intermediate in forming purine nucleotides via inosine-5-monophosphate
10	331.4	**deoxyadenosine monophosphate**	HMDB0000905	overexpression in cancer cells
11	335.4	fructose 1,6-bisphosphate	HMDB0003973	hyperactivity of glycolysis
12	347	adenosine monophosphate	HMDB0000045	overexpression
13	353.9	(2*S*,4*R*,5*S*)-4,5,6-trihydroxy-2-[hydroxyl (phosphonooxy) phosphoryl]oxy-3-oxohexanoic acid	HMDB0260134	part of human exposome
14	379.24	**sphingosine**1-phosphate	HMDB0000277	S1P controls numerous aspects of cell physiology, survival, and mammalian inflammatory responses
15	391	phosphoribosyl pyrophosphate	HMDB0000280	it was formed from ribose 5-phosphate by the enzyme ribose-phosphate diphosphokinase; it has a role in transferring phosphate groups.
16	427.21	adenosine diphosphate (ADP)	HMDB0001341	glucose metabolism
17	506.9	adenosine 5′-triphosphate (ATP)	HMDB0000538	hyperactivity of glycolysis
18	509.3	LysoPE (20:0/0:0)	HMDB0011515	sphingosine-1-phosphate (S-1-P) and lysophosphatidylcholine (lysoPC 17:0) are upregulated in HCC sera
19	523.5	guanosine triphosphate (GTP)	HMDB0001273	elevated intensity in cancer
20	531	PA (2:0/PGJ2)	HMDB0266517	oxidized phosphatidic acids belong to a group of biomolecules having a role as signaling molecules
21	549.3	LysoPC (20:1(11Z)/0:0)	HMDB0010391	overexpressed, potential biomarker, lipid metabolism
22	578.3	phosphatidic acid (10:0/17:0)	HMDB0114774	intermediates in the biosynthesis of triacylglycerols and phospholipids
23	648.8	PA (16:0/16:0)	HMDB0000674	biosynthesis of triacylglycerols and phospholipid
23	683.4	phosphatidylethanolamine (32:4)	HMDB0008832	elevated levels of cancer
24	745.4	NADPH	HMDB0000221	hyperactivity of glycolysis
25	787.1	**FADH**	HMDB0001197	hyperactivity of glycolysis

[a]Monoisotopic mass, HMDB ID, metabolic pathway information, and a link to cancer/exosomes are provided. The Human Metabolome Database (HMDB) is explored to identify the enriched metabolites

https://doi.org/10.1021/acsomega.3c08610
ACS Omega 2024, 9, 31335−31343

response to cancer, characteristic phosphometabolites contribute to altered glycolysis, lipid metabolism, and glutamine addiction. MALZ-based detection using SPE followed by LC−MS is developed to separate and profile phosphorylated metabolites from serum samples. A comparison of the metabolite control (Figure S3) and cancer sample (Figure 4) shows different metabolic MS profiles having 26 metabolites, including fucose 1-phosphate, glucose 6-phosphate, glyceric acid 1,3-biphosphate, fructose 1,6-bisphosphate, adenosine monophosphate, ADP, ATP, NADPH, and FADH. They are overexpressed in cancer, contribute toward high glycolysis, and are an exhaustive energy source for cancer cells.

Phospholipids such as sphingosine 1-phosphate LysoPE (20:0/0:0), LysoPC (20:1(11Z)/0:0), phosphatidic acid (10:0/17:0), and phosphatidyl ethanolamine (32:4) belong to lipid metabolism, and their expression is linked to cancer. Table 1 lists detected phosphometabolites from cancer serum samples, HMDB ID, m/z, and involved metabolic pathways.

Serum-derived metabolic profiles complement protein cancer biomarkers; however, the phosphometabolite content remains under-researched. This work aims to compare phosphometabolite profiles of cancer patients and healthy controls and observe the difference between normal and altered levels.

4. CONCLUSIONS

Phosphometabolites play a role in altered glycolysis and lipid metabolism in cancer. In this study, ternary hydroxides of magnesium, aluminum, and lanthanum loaded onto the porous zeolite (MALZ) are fabricated and optimized for the selective separation of phosphometabolites from serum and identified via LC−MS. Lanthanum, because of its acidic nature, possesses a higher affinity for phosphate, and compared to other transition metals, it shows a prominent role in phosphoproteomics. The utilization of magnesium and aluminum further enhances the affinity for the phosphate. MS profiles of malignant neoplastic and healthy serum samples show differences in the number and expression of phosphometabolites. MALZ with nanodiameter, homogeneous surface morphology, high surface area, available hydroxyl groups, and high affinity to phosphate groups offers SPE separations for phosphometabolite profiling in cancer-based studies.

■ ASSOCIATED CONTENT

Supporting Information

The Supporting Information is available free of charge at https://pubs.acs.org/doi/10.1021/acsomega.3c08610.

Materials and chemicals for MALZ synthesize; parameter optimization; adsorption kinetics of MALZ at initial AMP and ATP concentrations: (A) pseudo-first-order, (B) intraparticle diffusion, and (C) pseudo-second-order (Figure S1); mechanism of phosphate adsorption in acidic conditions (Figure S2); and MS profile of enriched metabolites from healthy serum sample by MALZ via SPE followed by LC−MS (Figure S3) (PDF)

■ AUTHOR INFORMATION

Corresponding Authors

Batool Fatima − *Department of Biochemistry, Bahauddin Zakariya University, Multan 60800, Pakistan;* orcid.org/0000-0003-3877-5090; Email: batoolfatima@bzu.edu.pk

Muhammad Najam-ul-Haq − *Institute of Chemical Sciences, Bahauddin Zakariya University, Multan 60800, Pakistan;* orcid.org/0000-0002-2090-5072; Email: najamulhaq@bzu.edu.pk

Authors

Tasbiha Malik − *Department of Biochemistry, Bahauddin Zakariya University, Multan 60800, Pakistan*

Dilshad Hussain − *HEJ Research Institute of Chemistry, International Center for Chemical and Biological Sciences, University of Karachi, Karachi 75270, Pakistan;* orcid.org/0000-0001-6187-5626

Fahmida Jabeen − *Institute of Chemical Sciences, Bahauddin Zakariya University, Multan 60800, Pakistan*

Shan E Zahra Jawad − *Department of Biochemistry, Bahauddin Zakariya University, Multan 60800, Pakistan*

Abrar Mohyuddin − *Department of Chemistry, The Emerson University Multan, Multan 60000, Pakistan*

Complete contact information is available at: https://pubs.acs.org/10.1021/acsomega.3c08610

Notes

The authors declare no competing financial interest.

■ ACKNOWLEDGMENTS

The authors acknowledge the Higher Education Commission (HEC) of Pakistan.

■ REFERENCES

(1) Kim, S.-Y. Cancer energy metabolism: shutting power off cancer factory. *Biomolecules & Therapeutics* **2018**, *26* (1), 39.

(2) Motolani, A.; et al. Phosphorylation of the regulators, a complex facet of NF-κB signaling in cancer. *Biomolecules* **2021**, *11* (1), 15.

(3) Cao, W.; et al. AMP-activated protein kinase: a potential therapeutic target for triple-negative breast cancer. *Breast Cancer Res.* **2019**, *21* (1), 1−10.

(4) Kim, J. Peroxisome metabolism in cancer. *Cells* **2020**, *9* (7), 1692.

(5) Naffouje, R.; et al. Anti-tumor potential of IMP dehydrogenase inhibitors: a century-long story. *Cancers* **2019**, *11* (9), 1346.

(6) Hoang, L. T.; et al. Metabolomic, transcriptomic and genetic integrative analysis reveals important roles of adenosine diphosphate in haemostasis and platelet activation in non-small-cell lung cancer. *Molecular oncology* **2019**, *13* (11), 2406−2421.

(7) Anwanwan, D.; et al. Challenges in liver cancer and possible treatment approaches. *Biochimica et Biophysica Acta (BBA)-Reviews on Cancer* **2020**, *1873* (1), No. 188314.

(8) Kudo, Y.; et al. PKCλ/ι loss induces autophagy, oxidative phosphorylation, and NRF2 to promote liver cancer progression. *Cancer Cell* **2020**, *38* (2), 247−262.

(9) Liu, G.; et al. Sorafenib kills liver cancer cells by disrupting SCD1-mediated synthesis of monounsaturated fatty acids via the ATP-AMPK-mTOR-SREBP1 signaling pathway. *FASEB J.* **2019**, *33* (9), 10089−10103.

(10) Wu, L.; et al. Rhein reverses doxorubicin resistance in SMMC-7721 liver cancer cells by inhibiting energy metabolism and inducing mitochondrial permeability transition pore opening. *BioFactors* **2019**, *45* (1), 85−96.

(11) Yuen, V.W.-H.; Wong, C.C.-L. Hypoxia-inducible factors and innate immunity in liver cancer. *J. Clin. Invest.* **2020**, *130* (10), 5052−5062.

(12) Puckett, D. L.; et al. The role of PKM2 in metabolic reprogramming: insights into the regulatory roles of non-coding RNAs. *International Journal of Molecular Sciences* **2021**, *22* (3), 1171.

(13) Fiorillo, M.; et al. High ATP production fuels cancer drug resistance and metastasis: Implications for mitochondrial ATP depletion therapy. *Front. Oncol.* **2021**, *11*, 3875.
(14) Sadik, A. Phosphometabolite Enrichment With Metal Oxide Microtips and Purification of Albumin From Canine Plasma. 2019, Saint Louis University.
(15) Qiu, W.; et al. Phosphopeptide enrichment for phosphoproteomic analysis-a tutorial and review of novel materials. *Anal. Chim. Acta* **2020**, *1129*, 158−180.
(16) Najam-ul-Haq, M.; et al. Alumina nanocomposites: a comparative approach highlighting the improved characteristics of nanocomposites for phosphopeptides enrichment. *Amino Acids* **2016**, *48* (11), 2571−2579.
(17) Veerasingam, M.; Murugesan, B.; Mahalingam, S. Ionic liquid mediated morphologically improved lanthanum oxide nanoparticles by Andrographis paniculata leaves extract and its biomedical applications. *Journal of Rare Earths* **2020**, *38* (3), 281−291.
(18) Wang, R.; et al. A "One-Stop Shop" Decision Tree for Diagnosing and Phenotyping Polycystic Ovarian Syndrome on Serum Metabolic Fingerprints. *Adv. Funct. Mater.* **2022**, *32* (45), No. 2206670.
(19) Li, Y.; et al. Bionanoparticles in cancer imaging, diagnosis, and treatment. *View* **2022**, *3* (4), No. 20200027.
(20) Yang, J.; et al. Defective Fe Metal−Organic Frameworks Enhance Metabolic Profiling for High-Accuracy Diagnosis of Human Cancers. *Adv. Mater.* **2022**, *34* (26), No. 2201422.
(21) Huang, Y.; et al. Diagnosis and prognosis of breast cancer by high-performance serum metabolic fingerprints. *Proc. Natl. Acad. Sci. U. S. A.* **2022**, *119* (12), No. e2122245119.
(22) Shi, W.; Fu, Y.; Jaing, W.; Ye, Y.; Kang, J.; Liu, D.; Ren, Y.; Li, D.; Lio, C.; Xu, Z. Enhanced phosphate removal by zeolite loaded with Mg-Al-La ternary(hydr)oxides from aqueous solutions: Performance and mechanism. *Chem. Eng. J.* **2019**, 33.
(23) Shi, W.; et al. Enhanced phosphate removal by zeolite loaded with Mg−Al−La ternary (hydr)oxides from aqueous solutions: Performance and mechanism. *Chemical Engineering Journal* **2019**, *357*, 33−44.
(24) Saravani, H.; Khajehali, M. Synthesis and characterization of Lanthanum oxide and lanthanumoxid carbonate nanoparticles from thermalizes of [La(acacen)(NO3)(H2O) complex. *Orient. J. Chem.* **2016**, *32*, 491−498.
(25) D'Haese, P. C.; et al. Human health risk associated with the management of phosphorus in freshwaters using lanthanum and aluminium. *Chemosphere* **2019**, *220*, 286−299.
(26) Xia, M.; et al. Synthesis and phosphate adsorption behaviour of Mg/Al-pillared montmorillonite loaded with La(OH)3. *Environ. Technol.* **2019**, 1652−1668.
(27) Li, M.; et al. Phosphate adsorption on metal oxides and metal hydroxides: A comparative review. *Environmental Reviews* **2016**, *24* (3), 319−332.
(28) Tarmahi, M. H.; Moeinpour, F. Phosphate removal from Aqueous solutions using Polyaniline/ NI0. 5ZN0. 5FE2O4Magnetic Nanocomposite. *Environ. Health Eng. Manage. J.* **2017**, *4* (2), 65.
(29) Iqbal, M. J.; Ashiq, M. N. Adsorption of dyes from aqueous solutions on activated charcoal. *J. Hazard Mater.* **2007**, *139* (1), 57−66.
(30) Mansouriieh, N.; Sohrabi, M. R.; Khosravi, M. Adsorption kinetics and thermodynamics of organophosphorus profenofos pesticide onto Fe/Ni bimetallic nanoparticles. *International Journal of Environmental Science and Technology* **2016**, *13* (5), 1393−1404.
(31) Omari, H.; et al. Study of the Phosphorus Adsorption on the Sediments. *J. Chem.* **2019**, *2019*, No. 2760204.

https://doi.org/10.1021/acsomega.3c08610
ACS Omega 2024, 9, 31335−31343